ACCELERATED DYNAMIC MRI USING SELF EXPRESSIVENESS PRIOR

Arvind Balachandrasekaran, Mathews Jacob

Electrical and Computer Engineering ,The University of Iowa,Iowa City,IA, USA

ABSTRACT

We introduce a self-expressiveness prior to exploit the redundancies between voxel profiles in dynamic MRI. Specifically, we express the temporal profile of each voxel in the dataset as a sparse linear combination of temporal profiles of other voxels. This scheme can be thought of as a direct approach to exploit the inter-voxel redundancies as opposed to low-rank and dictionary based schemes, which learn dictionaries from the data to represent the signal. The proposed representation may be interpreted as a union of subspaces model or as an analysis transform. The use of this algorithm is observed to considerably improve the recovery of myocardial perfusion MRI data from under sampled measurements.

Index Terms— Self Expressiveness, Analysis Transform, Union of Subspaces, Dynamic MRI reconstuction, Alternating minimization.

1. INTRODUCTION

The recovery of MRI data from under sampled measurements is critical to achieving high spatio-temporal resolution and spatial coverage in a variety of dynamic imaging problems. Low-rank and dictionary learning methods have been introduced to exploit the redundancy between the temporal profiles of the voxels of the dataset to make its recovery from highly under sampled data well-posed. These schemes learn the basis sets or dictionaries of temporal basis functions, which are representative of the voxel profiles, from the under sampled data. Since the estimated basis functions are considerably more efficient in representing the signal, these schemes provide significant performance improvement over methods which use pre-defined dictionaries. Specifically, the motion patterns and the physiological signal variations of different organs which are drastically different are captured by the representation.

The above approach of learning a dictionary and then using it to exploit the similarity between the voxel intensity profiles may be seen as an indirect approach. In this paper, we propose to directly exploit the redundancy between the voxel profiles. Specifically, we propose to express each voxel profile as a sparse weighted linear combination of other voxel profiles in the image. This translates to the constraint $\mathbf{S} = \mathbf{QS}$, where each row of $\mathbf{S}$ is the temporal profile of a specific voxel and $\mathbf{Q}$ is the weight matrix. The sparsity penalty on $\mathbf{Q}$ enables the selection of appropriate neighbors which are ideally suited to represent the specific voxel profile. This approach is inspired by sparse subspace clustering [1], where the estimation of the sparse $\mathbf{Q}$ is shown to be equivalent to fitting a union of subspaces model for $\mathbf{S}$. Specifically, every data point is represented as a linear combination of datapoints in the same subspace. While the union of subspaces (UoS) model has similarities to dictionary models [2], it is known to provide better representations . We term the property $\mathbf{S} = \mathbf{QS}$ as the Self Expressiveness Property (SEP). In the context of dynamic MRI, we propose to jointly estimate the data $\mathbf{S}$ and the weights $\mathbf{Q}$ from the under sampled measurements.

We employ an alternating minimization algorithm to jointly estimate $\mathbf{S}$ and the weights $\mathbf{Q}$ from the under sampled measurements. The dimension of the square weight matrix $\mathbf{Q}$ is equal to the number of voxels in the dataset. The large dimensionality of the weight matrix results in an algorithm whose computational complexity is prohibitively high. In imaging problems, the temporal profile of a specific voxel is more likely to be well represented in terms of its neighbors. We exploit this prior knowledge, and constrain Q to have the aforementioned structure to obtain a computationally feasible algorithm. Specifically, the temporal profile of each voxel is expressed as a sparse linear combination of the temporal profiles of voxels in a $p \times p$ neighborhood around the specific voxel. Similar approaches have been used in non-local regularization algorithms to keep the computational complexity of searches tractable [3, 4].

The above approach implies that the matrix $\mathbf{\Omega} = \mathbf{I} - \mathbf{Q}$ annihilates $\mathbf{S}$; i.e., $\mathbf{\Omega S} \approx 0$. Thus, the proposed scheme may also be viewed as an analysis transform learning scheme [5]. The optimization scheme learns a sparse analysis dictionary $\mathbf{\Omega}$ and data $\mathbf{S}$ from the undersampled measurements; the proposed scheme can be viewed as an extension to Blind Compressed Sensing (BCS) scheme [6] which jointly learns a synthesis dictionary and its sparse coefficients. Each row of $\mathbf{\Omega}$ can be interpreted as a $p \times p$ filter which annihilates the neighborhood of the corresponding voxel. Note that the use of the sparsity prior attenuates the filter coefficients correspond-

This work is in part supported by US NSF grants CCF-1116067, NIH 1R21HL109710-01A1, ACS RSG-11-267-01-CCE, and ONR grant N00014-13-1-0202.

ing to voxels in the neighborhood which are not similar to the specific voxel; the use of spatially varying filters which are optimized for each neighborhood is expected to provide considerably improved results over using fixed filters (e.g. gradient priors).

We determine the utility of the proposed formulation in the context of recovering myocardial perfusion MRI data from highly under sampled measurements. We compare the proposed scheme against the BCS scheme [6]; the comparisons show that the proposed scheme is capable of providing accurate reconstructions and minimizing spatio-temporal blurring.

2. THEORY

2.1. Problem Formuation

Let $\mathbf{S} \in \mathbb{C}^{\mathbf{M}\times\mathbf{t}} = [\mathbf{s}_1, \mathbf{s}_2, \ldots, \mathbf{s}_t]$ represent the Dynamic Magnetic Resonance Images (DMRI), where each $\mathbf{s}_i$ or the column of $\mathbf{S}$ represents an image frame and the rows represent voxel time profiles. We model the measurements as

$$\mathbf{b}_i = \mathbf{A}_i\,\mathbf{s}_i + \eta_\mathbf{i} \tag{1}$$

Here $\mathbf{A}_i \in \mathbb{C}^{\mathbf{L}\times\mathbf{M}}$; $\mathbf{L} \leq \mathbf{M}$ is the linear Fourier Undersampling Operator and η_i is the noise vector corresponding to the i^{th} measurement. Since equation (1) is under- determined, $\mathbf{s}_i$ cannot be recovered from the measurements $\mathbf{b}_i$.Hence constraints are introduced to make the problem well posed.

Since we assume the voxel profiles to lie in a union of low dimensional subspaces, we can use the self expressiveness property (SEP) of the data $\mathbf{S}$ as a prior. Mathematically SEP can be defined as

$$\mathbf{S} = \mathbf{Q}\,\mathbf{S} \tag{2}$$

where $\mathbf{Q} \in \mathbb{C}^{\mathbf{M}\times\mathbf{M}}$ is a weight matrix. In (2), every voxel time profile could have many representations in terms of other voxel time profiles and in general the representations are not unique. In this paper, we look for the sparsest representation, which ideally expresses every voxel time profile as a sparse combination of the temporal profiles of the voxels from its own subspace. We formulate the objective function as a linear combination of data consistency term and constraints.

$$\{\mathbf{S},\mathbf{Q}\}^* = \arg\min_{\mathbf{S},\mathbf{Q}} \|\mathcal{A}(\mathbf{S}) - \mathbf{b}\|_F^2 + \mu\,\|\mathbf{Q}\|_{\ell_1} \quad \text{such that} \quad \mathbf{S} = \mathbf{Q}\mathbf{S} \quad \text{and} \quad \mathrm{diag}(\mathbf{Q}) = \mathbf{0} \tag{3}$$

where μ is a regularizing parameter and $\mathrm{diag}(\mathbf{Q}) = \mathbf{0}$ is necessary to avoid the trivial solution of $\mathbf{Q} = \mathbf{I}$ in (2).

2.2. Constraining the weight matrix

In DMRI, the dimension of each column of $\mathbf{S}$ is very high. For example,when $\mathbf{S}$ is 16384×50 the size of $\mathbf{Q}$ is 16384×16384. Such a $\mathbf{Q}$ matrix demands a lot of memory for storage and increases the computational complexity of the problem. Thus the problem becomes intractable for large data sets and equation (3) becomes very difficult to solve.

We alleviate the problem by imposing a structure on Q. Specifically, we aim to represent the temporal profile of each voxel as a sparse combination of the temporal profiles of neighboring voxels in a window of size $\mathbf{p}\times\mathbf{p}$ around the specific voxel. This choice is motivated by the prior knowledge that the temporal profiles of nearby voxels are most likely similar. This choice reduces the number of non-zero entries in every row of $\mathbf{Q}$ to (p^2-1). Hence, the maximum number of unknowns to be solved in $\mathbf{Q}$ has reduced from $\mathbf{M}^2$ to $\mathbf{M}\,(p^2-1)$, which is computationally tractable.

2.3. Optimization Algorithm

In order to solve equation (3), we introduce an auxiliary variable $\mathbf{P}$ and relax the $\mathbf{S} = \mathbf{Q}\mathbf{S}$ constraint by adding it in the objective function. The modified cost function becomes

$$\{\mathbf{S},\mathbf{P},\mathbf{Q}\}^* = \arg\min_{\mathbf{S},\mathbf{P},\mathbf{Q}} \|\mathcal{A}(\mathbf{S}) - \mathbf{b}\|_F^2 + \mu(\|\mathbf{P}\|_{\ell_1} + \lambda\|\mathbf{S} - \mathbf{Q}\mathbf{S}\|_F^2) \quad \text{such that} \quad \mathbf{Q} = \mathbf{P} \text{ and } \mathrm{diag}(\mathbf{Q}) = \mathbf{0} \tag{4}$$

We add the constraint $\mathbf{Q} = \mathbf{P}$ as a penalty for simplicity and rewrite (4) as the following optimization program.

$$\{\mathbf{S},\mathbf{P},\mathbf{Q}\}^* = \arg\min_{\mathbf{S},\mathbf{P},\mathbf{Q}} \|\mathcal{A}(\mathbf{S}) - \mathbf{b}\|_F^2 + \mu(\|\mathbf{P}\|_{\ell_1} + \lambda\|\mathbf{S} - \mathbf{Q}\mathbf{S}\|_F^2 + \frac{\beta}{2}\|\mathbf{Q} - \mathbf{P}\|_F^2) \text{ such that } \mathrm{diag}(\mathbf{Q}) = \mathbf{0} \tag{5}$$

where λ is a regularizing parameter and β is a penalty parameter. We employ an alternating minimization scheme to solve equation (5), where the optimization is done over one variable keeping the other two variables fixed. This results in the following sub problems.

$$\mathbf{P_{n+1}} = \arg\min_{\mathbf{P}} \|\mathbf{P}\|_{\ell_1} + \frac{\beta}{2}\|(\mathbf{Q_n} - \mathbf{P})\|_F^2 \tag{6}$$

$$\mathbf{Q_{n+1}} = \arg\min_{\mathbf{Q}} \lambda\|\mathbf{S}_n - \mathbf{Q}\mathbf{S}_n\|_F^2 + \frac{\beta}{2}\|(\mathbf{Q} - \mathbf{P_{n+1}})\|_F^2 \text{ such that } \mathrm{diag}(\mathbf{Q}) = \mathbf{0} \tag{7}$$

$$\mathbf{S_{n+1}} = \arg\min_{\mathbf{S}} \|\mathcal{A}(\mathbf{S}) - \mathbf{b}\|_F^2 + \mu\lambda\|\mathbf{S} - \mathbf{Q_{n+1}}\mathbf{S}\|_F^2 \tag{8}$$

Equation (6) can be solved analytically using an L_1 shrinkage on each element of $\mathbf{Q}$ as

$$\mathbf{P_{n+1}} = \frac{\mathbf{Q_n}}{|\mathbf{Q_n}|}\left(|\mathbf{Q_n}| - \frac{1}{\beta}\right)_+ \tag{9}$$

where '+' is the shrinkage operator defined as $\tau_+ = \max\{0, \tau\}$.

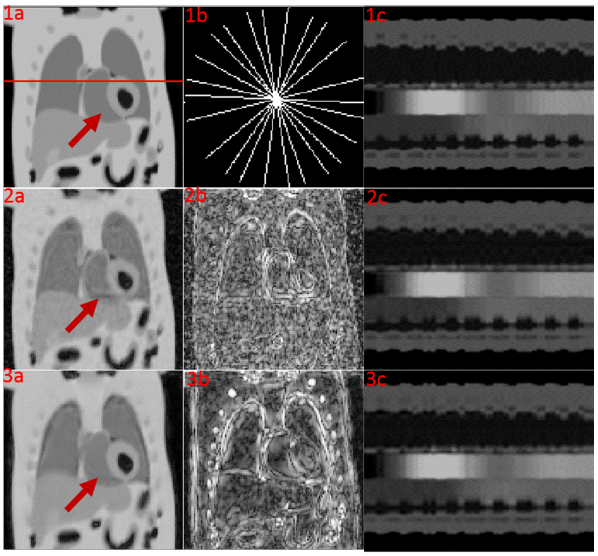

Fig. 1: Comparison of the proposed formulation with BCS on the PINCAT phantom. 1a, 2a, 3a represent a frame from ground truth, BCS reconstruction and the proposed scheme respectively. A sampling mask with 12 lines is shown in 1b. This mask is rotated by the golden angle for each image frame. The scaled (x10) error images for BCS and the proposed formulation are depicted in 2b and 3b respectively. The last column represents the image time profile along the red line shown in 1a. The Signal to Error (SER) of the reconstructions from BCS and the proposed algorithm are 25.1 dB and 25.27 dB respectively.

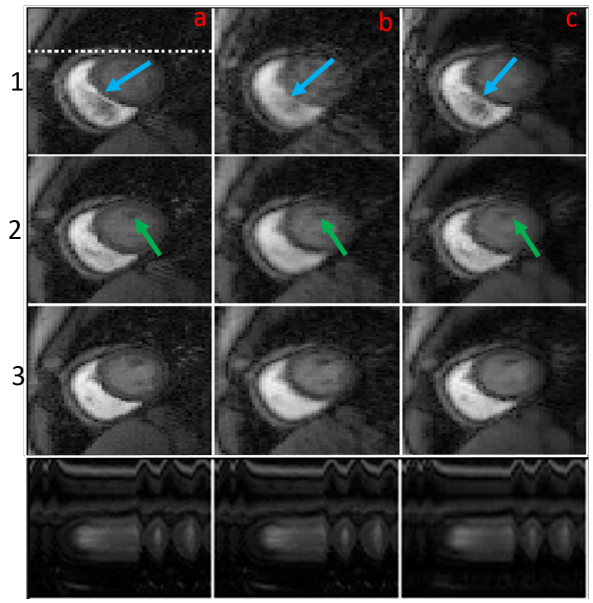

Fig. 2: Comparison of the proposed formulation with BCS on the Myocardial Perfusion Dataset. 1a, 2a and 3a represent the frames of the original data set. The frames under b and c are reconstructed using BCS and the proposed scheme respectively. The last row represents the time profile along the white line in 1a. The Signal to Error (SER) of the reconstructions from BCS and the proposed algorithm are 13.58 dB and 14.08 dB respectively.

Since $\mathbf{Q}$ has $(\mathbf{M}(p^2-1))$ entries and the location of non-zero entries in each row are determined based on the window around the specific voxel, an analytical expression is obtained for the $\mathbf{i}^{th}$ row of equation (7), which is then used to update the rows of $\mathbf{Q}$. Equation (8) is a quadratic problem; we solve it using the Conjugate Gradient (CG) algorithm.

We employ a continuation strategy to solve the sub problems. We have two loops - an inner and and outer loop. We start with a small value of β in the outer loop and alternate between the sub problems in the inner loop until the difference in the cost of (3) over successive inner iterations is below a threshold. After this, we increment β and alternate between the sub problems again. The algorithm is terminated once the cost of (3) over successive outer iterations is below a threshold.

3. RESULTS

We compare the performance of the proposed algorithm against the BCS scheme [6] in recovering the Physiologically Improved Non uniform CArdiac Torso (PINCAT) phantom [7], set to simulate myocardial perfusion imaging data (MPI), as well as experimentally acquired MPI data. In order to reduce the memory demand of $\mathbf{Q}$, we consider a 7x7 window around every voxel and express its temporal profile as a sparse

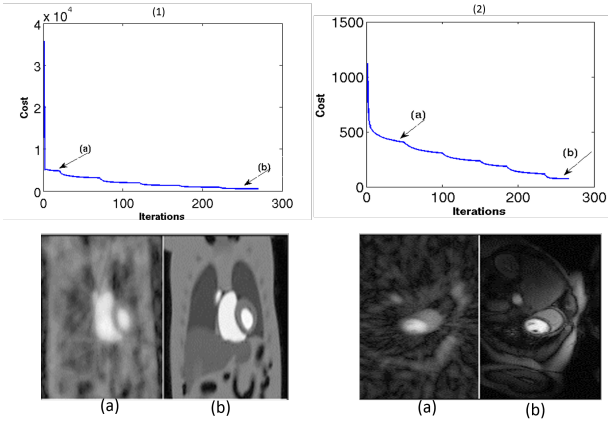

Fig. 3: (1) and (2): Cost of (3) vs Iteration for the proposed scheme on PINCAT and Myocardial Perfusion data respectively. A continuation scheme is employed to solve (3), where we start with a small β value and increment it every few iterations. (a) and (b) are reconstructed frames corresponding to small and high β values respectively.

linear combination of the temporal profiles of other voxels in this window. Hence, the maximum number of non-zero elements in each row of $\mathbf{Q}$ is 48.

3.1. Simulation Results

We consider 50 frames of the PINCAT phantom of spatial dimension 128x128 for comparing the proposed formulation with the BCS algorithm. The phantom is undersampled using a golden angle trajectory interpolated on a Cartesian grid.The golden angle is equal to 111.25 degrees, which is the angle between consecutively acquired radial lines of kspace. We construct each frame of the phantom using 12 lines, which corresponds to an acceleration factor of 9.7. One frame of the sampling mask is shown in Fig.1.b.

We compare the proposed formulation with the BCS algorithm on the PINCAT phantom in Fig.1. 1a, 2a and 3a of the first column correspond to the ground truth frame, images reconstructed from BCS and the proposed formulation respectively. The reconstructed frame from the BCS algorithm suffers from artifacts, especially in the region pointed by the red arrow. These artifacts are considerably suppressed in the frame reconstructed by the proposed scheme.In the presence of artifacts, the temporal profiles of voxels in the region are quite dissimilar and hence the use of sparsity prior annihilates small coefficients of the $\mathbf{Q}$ matrix resulting in the suppression of artifacts.The error images for BCS and the proposed formulation are shown in 2b and 3b of second column respectively. The image time profiles along the red line in 1a are shown in the last column.

3.2. Myocardial Perfusion Results

We compare the proposed scheme with the BCS algorithm on a retrospectively undersampled myocardial perfusion dataset of dimension 190x190x70 with motion at an acceleration factor of 7.5. The data set was acquired at the 3T Siemens MRI scanner at the University of Utah. The subject was at rest and a Gd bolus of 0.02 mmol/kg was administered. The pulse sequence used was a saturation recovery FLASH sequence with the following parameters :Slices=3,TR/TE=2.5/1.5 ms,saturation recovery time=100 ms. A uniform radial sampling trajectory with 12 lines was used for each frame and was randomly rotated for subsequent frames.

The comparison of the proposed formulation with BCS is shown in Fig.2. Three frames (1,2,3) are chosen for comparison and a, b and c represent the ground truth frame, reconstructed frames from BCS and the proposed formulations respectively. We observe that the region bordering the left and the right ventricle as indicated by the blue arrow, and the papillary muscles indicated by the green arrow, are more faithfully captured with the proposed algorithm. Since the voxels in a small neighborhood have similar temporal profiles, the proposed formulation expresses the temporal profile of a specific voxel in the border/edge as a sparse linear combination of temporal profiles of voxels in close proximity.This results in the faithful capture of the edges in the reconstruction. The final cost of (3) vs iterations is shown in Fig.3.

4. CONCLUSION

We introduced a self expressiveness prior for the recovery of dynamic MRI data from highly under sampled measurements. The redundancy between voxel profiles is exploited by expressing the temporal profile of a specific voxel as a sparse linear combination of temporal profiles of other voxels in a window of size $\mathbf{p} \times \mathbf{p}$ around the specific voxel . This enabled us to use the MRI data as the dictionary. An alternating minimization algorithm was employed to jointly estimate the weight matrix and the MRI data. The proposed formulation was compared with the BCS algorithm on the PINCAT phantom and the MPI data. The results showed that the reconstructions from the proposed formulation had fewer artifacts and also efficiently preserved the borders and structural details.

5. REFERENCES

[1] Ehsan Elhamifar and Rene Vidal, "Sparse subspace clustering:algorithm, theory, and applications," *IEEE Transactions on Pattern Analysis and Machine Intelligence*, vol. 35, pp. 2765 – 2781, November 2013.

[2] Lihi Zelnik-Manor, Kevin Rosenblum and Yonina C. Eldar, "Dictionary optimization for block-sparse representations," *IEEE Transactions on Signal Processing*, vol. 60, pp. 2386 – 2395, May 2012.

[3] Zhili Yang and Mathews Jacob, "Nonlocal regularization of inverse problems: a unified variational framework," *IEEE Transactions on Image Processing*, vol. 22, pp. 3192 – 3203, August 2013.

[4] Joshua D. Trzasko, "Exploiting local low-rank structure in higher-dimensional mri applications," *Proceedings of SPIE*, vol. 8858, September 2013.

[5] Saiprasad Ravishankar and Yoram Bresler, "Doubly sparse transform learning with convergence guarantees," *Proceedings of ICASSP,Florence*, 2014.

[6] Sajan Goud Lingala and Mathews Jacob, "Blind compressive sensing dynamic mri," *IEEE Transactions on Medical Imaging*, vol. 32, pp. 1132–1145, June 2013.

[7] B. Sharif, Y. Bresler, "Physiologically improved ncat phantom (pincat) enables in-silico study of the effects of beat-to-beat variability on cardiac mr," *Proceedings of the Annual Meeting of ISMRM, Berlin*, 2007.